

# Magnetic penetration depth measurements of superconducting thin films by a microstrip resonator technique

B. W. Langley,<sup>a)</sup> S. M. Anlage,<sup>b)</sup> R. F. W. Pease,<sup>a)</sup> and M. R. Beasley  
*Department of Applied Physics, Stanford University, Stanford, California 94305*

(Received 1 March 1991; accepted for publication 2 April 1991)

The microstrip resonator technique is a convenient way to sensitively measure the temperature dependence of the magnetic penetration depth,  $\lambda(T)$ , in superconducting thin films. Because the method relies on measuring the resonant frequency of a microwave transmission line resonator, one can very precisely measure small changes in  $\lambda(T)$ . This technique can resolve changes in  $\lambda$  on the order of several angstroms, allowing a direct measurement of the low-temperature behavior of  $\lambda(T)$ , which is a measure of the low-lying pair breaking excitations of the superconductor. Absolute penetration depth values can also be obtained from a self-consistent fit to the data to an assumed temperature dependence. Measurements of the penetration depth of Nb and NbCN film give results that are consistent with the predictions of BCS theory in which  $2\Delta/kT_c$  is treated as an adjustable parameter, while  $\text{YBa}_2\text{Cu}_3\text{O}_{7-\delta}$  films give results that are not completely understood at this time. We also compare this technique with other methods of measuring the penetration depth of superconducting thin films, and discuss the systematic errors present in the measurement.

## I. INTRODUCTION

In response to an external magnetic field, a superconductor generates currents near its surface that shield out the applied field. The characteristic depth to which the shielding currents flow is the magnetic penetration depth  $\lambda$ . This penetration depth is temperature dependent, starting from a finite value,  $\lambda_0$ , at  $T = 0$  K, and increasing monotonically as  $T$  approaches  $T_c$  until the normal state skin depth dominates the electromagnetic response.

The penetration depth is sensitive to the properties of the superconductor near its surface, or in a film of thickness  $t < \lambda$ , to the entire film. The temperature dependence of the penetration depth is also sensitive to the nature of the quasiparticle excitation spectrum, since the penetration depth increases as the superconducting carrier density is depleted by thermal excitations. For instance, a superconductor with a nonzero energy gap over its entire Fermi surface will have an exponentially activated penetration depth temperature dependence at low temperatures, which is determined by the Boltzmann distribution of quasiparticles over its lowest energy gap. On the other hand, a superconductor with nodes in the energy gap will show a polynomial dependence for  $\lambda(T)$  at low temperatures since there is a continuous spectrum of quasiparticle excitations.<sup>1</sup> To distinguish between these two possibilities it is very important to determine the low-temperature dependence of  $\lambda(T)$  as accurately as possible. Also, at all temperatures  $1/\lambda^2$  is proportional to the square of the modulus of the superconducting order parameter, whose temperature dependence is sensitive to the magnitude of the gap  $2\Delta(0)/kT_c$ . Novel superconducting materials such as the heavy fermion, organic, and possibly copper-oxide classes

are thought to have nonconventional pairing symmetry, which could lead to a distinctive non-BCS temperature dependence of  $\Delta(T)$ . Thus, careful measurements of  $\lambda$  allows one to investigate the pairing state of such materials.<sup>2</sup>

Many methods have been used to measure the magnetic penetration depth in superconducting thin films. Naturally, most of these methods rely upon measuring the diamagnetic response of the superconductor. One of the most direct techniques involves measuring the magnetization of the sample as a function of temperature and applied field. In the normal state, a steady magnetic field will completely permeate a metal since the screening currents will eventually die out. In the superconducting state, however, the shielding currents will persist and the static magnetic field will be shielded out over a characteristic length  $\lambda$ , giving rise to a diamagnetic moment. Measurements of the diamagnetic susceptibility  $\chi_{dc} = M/H$  of a superconductor as a function of temperature, and knowledge of the sample geometry, allow one to calculate changes in  $\lambda$ . Absolute values of  $\lambda$  can then be obtained with the use of a theoretical, or independently measured, penetration depth temperature dependence  $\lambda(T)/\lambda(0)$ .<sup>3</sup> The advantage of this method lies in the fact that it is a direct measurement of the magnetic properties of the material. On the other hand, the detailed morphology and dimensions of the sample must be known in order to calculate the magnitude of the penetration depth. Single crystal samples with a simple geometry prove to be the most reliable way of determining the magnetic penetration depth by magnetization.<sup>4</sup>

One can also determine  $\lambda$  by measuring the ac susceptibility  $\chi_{ac} = dM/dH$  obtained when an alternating magnetic field is applied to the sample. The ac susceptibility is

<sup>a)</sup>Also at Stanford Electronics Laboratory, Stanford University.

<sup>b)</sup>Present address: Physics Department, Center for Superconductivity Research, University of Maryland, College Park, Maryland 20742.

simply related to the magnetization of the sample, and similar considerations as above apply to the extraction of  $\lambda$  from the data. The measurement is often done by placing one or more pickup coils around the sample and measuring their self or mutual inductance. This technique was originally employed by Schawlow and Devlin to study the penetration depth in superconducting tin.<sup>5</sup> Sridhar, Wu, and Kennedy<sup>6</sup> have used this technique to measure the magnetic field dependence of  $\lambda$  in single crystal  $\text{YBa}_2\text{Cu}_3\text{O}_{7-\delta}$ .

Another method that makes use of the inductance of a superconductor is the mutual inductance technique.<sup>7,8</sup> A superconducting film is positioned such that it modifies the mutual inductance of a pair of coils. The coils are wound astatically to confine the magnetic field and eliminate the effects of stray external field and pickup. One coil is driven at kilohertz frequencies and the pickup voltage in the receive coil is monitored by phase-sensitive detection. The in-phase and quadrature signals can be analyzed to yield the transverse penetration depth  $\lambda^2/d$  ( $d$  is the film thickness) and the dissipation. The technique has been used to study the penetration depth in high- $T_c$  thin films and the Kosterlitz–Thouless transition in type-II superconductors.<sup>9</sup> Quantitative interpretation of the data relies upon a calculation of the current distribution induced in the film by the drive coil,<sup>8</sup> as well as knowledge of the coil dimensions and spacings. The film must be thin compared to  $\lambda$  and very homogeneous to measure the low temperature dependence of  $\lambda$ . Flux pinning can also affect the result.

Another measurement technique, which has traditionally been used to study the surface impedance of superconductors at microwave frequencies, is the resonant cavity. Cavity walls can be coated with a superconductor to a few penetration depths in thickness,<sup>10</sup> or the entire cavity can be made from the material of interest.<sup>11</sup> Alternatively, a superconducting thin film can be used as an end plate for a cylindrical or rectangular cavity,<sup>12</sup> or the superconductor can be placed in a high rf magnetic field region inside the cavity.<sup>13,14</sup> The resonant frequency of the cavity is influenced by the penetration depth of the superconductor through the cavity inductance. Also, the  $Q$  of the cavity resonance is influenced by the superconducting losses. Thus the shift in resonant frequency of the cavity as a function of temperature can be used to determine changes in the penetration depth of the superconductor.<sup>15</sup> Here again, a determination of the absolute value of  $\lambda$  is considerably more difficult. In addition, if the superconducting film is thin compared to  $\lambda$ , the measurement is sensitive to the effective microwave impedance of the region behind the superconducting film.<sup>16–18</sup>

All of the measurement techniques mentioned above have limitations, particularly in the determination of  $\lambda(T)$  at low temperatures. In measurements of the thin film susceptibility, as well as mutual inductance, resolution suffers when the film is completely shielding; these techniques measure only noise in the system one the film is in the saturated shielding state. The Schawlow–Devlin technique also suffers from nonlinearities in the background at low temperatures,<sup>18</sup> while resonant cavities are limited by their finite sensitivity to the sample inductance. In this article we

describe a simple technique that gives a very high resolution penetration depth measurement, particularly at low temperatures where other techniques fail. The technique is based on measurements of the resonant frequency of a microstrip resonator constructed using superconducting thin films.

## II. PRINCIPLE OF THE MEASUREMENT

As seen above, a simple way to determine the magnetic penetration depth of a superconductor is to measure the inductance of the thin film. The inductance of a superconducting thin film is the sum of two parts, the magnetic inductance and the kinetic inductance. The magnetic inductance reflects the energy stored in magnetic fields created in the region around and inside the film due to currents in the film, and depends on the conductor geometry and the penetration depth. The kinetic inductance reflects the energy stored in the inertia of the superconducting carriers, and is proportional to  $\lambda^2$  divided by the cross sectional area of the film, for films thin compared to  $\lambda$ .<sup>20,21</sup> For suitable thin film geometries,<sup>20–23</sup> the kinetic inductance can be made large and very sensitive to  $\lambda$ . In fact, the present work grew out of the development of a kinetic inductance dominated variable delay transmission line for use at millimeter-wave frequencies.<sup>22</sup>

A direct measurement of the thin film inductance is difficult. A common technique to measure the inductance is to put the film into an electrical circuit and measure a

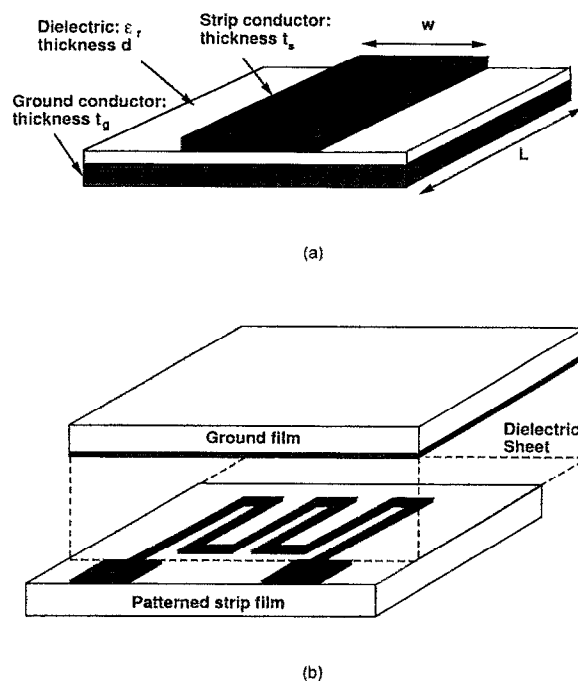


FIG. 1. (a) The microstrip transmission line geometry. The strip conductor has a thickness,  $t_s$ , a linewidth,  $w$ , and a penetration depth,  $\lambda_s$ . The ground plane has a thickness,  $t_g$ , and a penetration depth,  $\lambda_g$ . The dielectric has a thickness,  $d$ , and a dielectric constant  $\epsilon_r \epsilon_0$ . (b) The “flip-chip” implementation of the microstrip geometry, which is realized by clamping a dielectric sheet between an unpatterned ground plane film and a patterned strip film.

property of that circuit that depends on the inductance.<sup>5,23</sup> In this technique we measure the phase velocity of a microstrip transmission line [Fig. 1(a)] fabricated using superconducting thin films. The phase velocity for a signal propagating on a lossless transmission line is simply  $v_p = (LC)^{-1/2}$ , where  $L$  is the series inductance per unit length and  $C$  is the shunt capacitance per unit length. The inductance per unit length for a microstrip line is given by

$$L = (\mu_0/kw) [d + \lambda \coth(t_s/\lambda) + \lambda \coth(t_g/\lambda) + \lambda g_c \operatorname{csch}(t_g/\lambda)], \quad (1)$$

where  $w$  is the width of the strip film,  $t$  is the film thickness,  $d$  is the dielectric thickness, and the subscripts  $s$  and  $g$  refer

to signal and ground plane respectively (Fig. 1). The factors  $k$  and  $g_c$  take the fringing fields and ground/strip asymmetries of the two-dimensional microstrip geometry into account, and are obtained from formulas derived by Chang.<sup>24</sup> Note that we have assumed that the ground and strip superconducting films have the same penetration depth. The capacitance per unit length for a microstrip line is given by

$$C = \epsilon_{\text{eff}} \epsilon_0 (kw/d), \quad (2)$$

where the effective dielectric constant,  $\epsilon_{\text{eff}}$ , takes the multiple dielectric system of the microstrip geometry into account.<sup>25</sup> Hence the phase velocity for a lossless microstrip transmission line is given by

$$v_p = \frac{c/\sqrt{\epsilon_{\text{eff}}}}{\sqrt{1 + (\lambda/d) [\coth(t_s/\lambda) + \coth(t_g/\lambda) + g_c \operatorname{csch}(t_g/\lambda)]}}, \quad (3)$$

where  $c = (\epsilon_0 \mu_0)^{-1/2}$  is the speed of light in vacuum. Note that the phase velocity is independent of the factor  $k$ , but still has contributions from field fringing through  $\epsilon_{\text{eff}}$  and  $g_c$ . We have also investigated the effect of losses on the phase velocity of a superconducting microstrip line. We find that for typical measurement frequencies (1–10 GHz) and  $T < 0.98 T_c$ , the effect of losses on the phase velocity is negligible. A more detailed discussion of this can be found in Sec. V.

In practice, time domain measurements of the phase velocity of a transmission line are difficult to perform. However, the phase velocity can be easily measured as the resonant frequency of a finite section of transmission line which is terminated by large impedance mismatches. The resonance condition is that an integral number of half wavelengths span the transmission line's length,  $L$ . From this condition we see that the phase velocity is given by  $v_p = 2L f_n / n$ , where  $f_n$  is the  $n$ th resonant frequency. We have chosen  $L \approx 4$  cm so that the resonant frequencies are in the GHz range. Measuring the phase velocity in the frequency domain brings with it certain advantages. In particular, since microwave frequency sources can be obtained with stabilities of one part in  $10^9$ , a resonant frequency determination can potentially be done with very great precision. In practice, the resonant frequencies cannot be determined to one part in  $10^9$  because there is finite attenuation in the transmission line, leading to broadening of the resonance peaks. This broadening is proportional to the losses suffered by the microwave signal, so the resolution of the penetration depth measurement is higher for microstrips with lower losses. Consequently, the microstrip resonator method is well suited for measuring  $\lambda(T)$  in superconductors at low temperatures where the film losses are lowest.

The microstrip resonator measurement has its origins in the work of Pippard<sup>26</sup> who first suggested measuring the phase velocity of a signal propagating on a superconduct-

ing transmission line to determine the inductance and magnetic penetration depth of the materials. Young *et al.* were the first to use this technique to measure the penetration depth temperature dependence in thin films.<sup>27</sup> The technique was later adopted by Mason and Gould<sup>28</sup> to measure the penetration depth and coherence length in indium. Henkels and Kircher<sup>29</sup> used microstrip lines to measure the mean free path dependence of the penetration depth in Pb alloys. They also confirmed the thickness dependence of the effective penetration depth for films thin compared to the penetration depth,  $\lambda_{\text{eff}} = \lambda \coth(t/\lambda)$ . A method similar to this, but designed to measure surface resistance rather than inductance, has been successfully used to measure the surface resistance of high temperature superconducting films.<sup>30</sup>

### III. MICROSTRIP RESONATOR MEASUREMENT

The resonator measurement setup is shown in Fig. 2. First we will describe the sample probe that allows the microwave measurement of a resonator that is cooled to low temperatures. The probe consists of a 1.5-m-long thin-walled stainless steel tube with a probe tip attached to one end and a room-temperature connection box attached to the other. The probe tip is composed of two separable parts as shown in Fig. 2(b). The upper part of the probe tip is a dc terminal breadboard that is rigidly attached to the stainless steel probe tube and houses two single in-line package (SIP) strips, while the lower part of the probe is the sample platform. The pins of the SIPs are directly connected to BNC terminals on the room temperature connection box by means of small gauge copper wires running the length of the probe tube. Detachable electrical connections to the probe tip can then be made from the SIPs.

The microstrip transmission line is assembled in a "flip-chip" geometry [Fig. 1(b)] directly on the probe tip sample platform as shown in Fig. 2(b). In this geometry, two films are clamped together face to face, with a dielec-

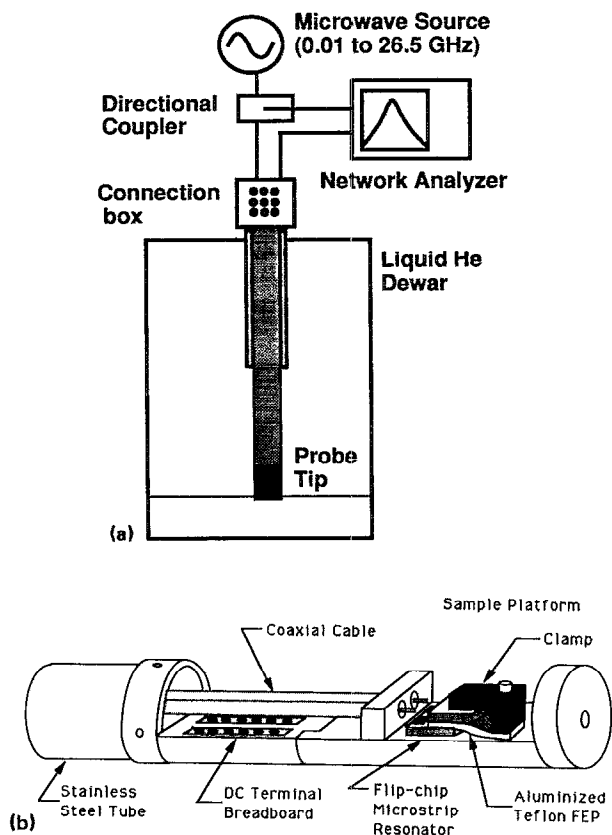


FIG. 2. (a) Schematic illustration of the low-temperature microwave measurement setup. (b) Here we see the probe tip in more detail. The "flip-chip" microstrip resonator is mounted on the sample platform.

tric sheet in between. One film is lithographically patterned with a long meandering line terminated with coupling pads, while the other film is left unpatterned to form the microstrip ground plane. We use two films with nominally identical penetration depths for a given microstrip resonator in order to simplify the data analysis. The two films are usually obtained from a larger sample that has been cut into 0.25 in. or 0.5 cm square samples. One could also use a superconductor that has a known penetration depth as the ground plane. We typically use mylar or Teflon FEP<sup>31</sup> sheets of  $\frac{1}{2}$  or 1 mil thickness, or thin (40–50  $\mu\text{m}$  thick) sapphire wafers for the dielectric. The dielectric sheets have a thin aluminum layer deposited on part of its surface in order to provide a ground contact between the back edge of the ground film surface (the top film in Fig. 2) and the Cu sample clamp. The dielectric sheet is not metallized over that part of its surface that forms the microstrip line. The "flip-chip" geometry results in a multiple dielectric medium that complicates the calculation of  $\epsilon_{\text{eff}}$ ; however the measurement results are independent of the dielectrics chosen. We originally fabricated our microstrip transmission lines in this geometry for two reasons. First of all, a monolithic microstrip structure was not possible since high quality multilayer films of high temperature superconductors are only now being realized.<sup>32</sup> Second, we wished to avoid degradation of the superconduction properties of our films due to excessive processing. Thus, we did not use

deposited dielectric layers. One advantage of the "flip-chip" geometry over monolithic structures or deposited dielectrics is that the dielectric thickness can be easily changed. Equation (3) shows that the temperature dependence of the phase velocity increases as the dielectric thickness decreases; thus, smaller dielectric thicknesses are preferred for penetration depth measurements.

As explained above, the microstrip transmission line can be assembled directly on the sample platform section of the probe tip (see Fig. 2). However, in a more recent implementation of this measurement technique, the microstrip samples are clamped together in a spring-loaded Cu sample holder, which is then mounted on the probe tip sample platform. This has several advantages over the previous method. First of all, the microstrip assemblies can be removed from the probe tip without breaking the flip-chip stack. Second, the Cu sample holder forms a minimum volume cavity around the microstrip transmission line that serves to raise the resonant frequencies of any spurious package resonances. Third, the springloaded clamping allows better control of strip film to ground film alignment. Last, and perhaps most important, the ground contact is now made via a thin metal sheet that is attached to the Cu sample holder and forms a springlike contact with the edge of the ground plane film. This ground contact is more reliable than the previous method, and eliminates the need to partially metallize the dielectric sheets.

The microstrip resonator is excited by microwave signals from a Hewlett Packard 8340B synthesized source, which are brought down to the sample platform by a low thermal conductivity stainless steel coax line (0.086 in. diameter). This same coax line also carries the microwave power reflected from the resonator to a directional coupler, which directs the signal to a Hewlett Packard 8757 Scalar Network Analyzer (SNA). Another identical coax line carries the power transmitted through the resonator from the sample platform to a microwave detector mounted on the top connection box, which directs the signal to the network analyzer. These coax lines are capacitively coupled to the microstrip input pads [Fig. 2(b)]. The lines are free to rotate and move in the longitudinal direction, and their position can be adjusted by moving them through Ultra-Torr fittings at the base of the connection box. This allows adjustment of the resonator coupling. The reflected and transmitted power signals are displayed as a function of frequency on the SNA.

In order to obtain the penetration depth of the superconducting films we must obtain reflected and transmitted power traces for temperatures ranging from as low as possible to  $T_c$ . Temperature control of the resonator can be done in one of two ways. For rapid characterization, the microwave probe can be directly inserted into a helium storage Dewar. The temperature of the sample is then controlled by raising or lowering the probe with respect to the liquid helium surface. However, this method proved to have undesirable side effects at the lowest temperatures due to the helium vapor. As the probe approaches the liquid helium surface, the vapor density changes rapidly, leading to temperature-dependent dielectric effects that can ob-

scure the effect of the temperature-dependent penetration depth. Because of this, a vacuum can was built to allow measurements in a low background pressure of helium. In this method the probe end is cooled by means of an exchange gas, which is subsequently pumped out. The temperature is then controlled over a broad range by means of a Lake Shore 91C temperature controller with a calibrated Si diode thermometer and a 25  $\Omega$  heater. In either method, electrical connections to Si diode thermometers, heaters, or dc bias leads can be made via the array of BNC connectors on the top connection box.

The measurement procedure is as follows. The sample is cooled slowly to the lowest measurement temperature. At this point, the coax lines are adjusted such that the coupling to the resonator is in the loose coupling limit. In this limit both the resonant frequency and resonance  $Q$  are independent of coupling strength. Note that loosening the coupling too much results in a reduction of the signal-to-noise ratio, making the measurement more difficult, especially at high temperatures where losses are greater. Experimentally we have observed that a resonator insertion loss (power incident on the resonator minus transmitted power) at low temperatures greater than 20 dB is necessary to ensure that the resonator is loosely coupled. The microwave power incident on the resonator is usually set at 0 dBm. When the microwave power is too high, the resonances are degraded by power-dependent losses.<sup>33,34</sup> Once the coupling is adjusted, the resonance that we wish to measure is centered in the SNA window, and the temperature is slowly increased using one of the methods outlined above. The reflected and transmitted power traces are transferred to a HP9000 series computer and stored in memory for as many as 500 temperature points.

The raw data consist of the reflected and transmitted power traces,  $P_R(f)$  and  $P_T(f)$ , for the temperatures measured. The resonant frequency and resonance  $Q$  is obtained from the transmitted power trace, which is fit to a skewed Lorentzian line shape that includes a linear background

$$P_T(f) = T_1 + T_2 f + \frac{T_3 + T_4 f}{1 + [(f - T_5)^2 / T_6]}$$

by a nonlinear least squares fitting routine. The resonant frequency is  $f_{\text{res}} = T_5$  and the resonance  $Q = T_5 / 2 \sqrt{T_6}$ . For an unskewed Lorentzian ( $T_2$  and  $T_4 = 0$ ) we can simply identify  $f_{\text{res}}$  as the frequency at the peak in the  $P_T(f)$  curve, and the resonance  $Q$  as  $f_{\text{res}} / \Delta f_{3 \text{ dB}}$ , where  $\Delta f_{3 \text{ dB}}$  is the difference in frequency between the two half power points of the resonance (relative to the peak power). Once the resonant frequency is determined for all of the measurement temperatures, a plot of phase velocity versus temperature for the microstrip line can be made (Fig. 3). Recall that the phase velocity is very simply related to the  $n$ th resonant frequency by the expression,  $v_p = 2L f_n / n$ , when in the loose coupling limit.

Note that since the resonance  $Q$  is inversely proportional to line losses, we can also use this technique to determine the microstrip line attenuation. However, obtaining the surface resistance of the superconducting thin films

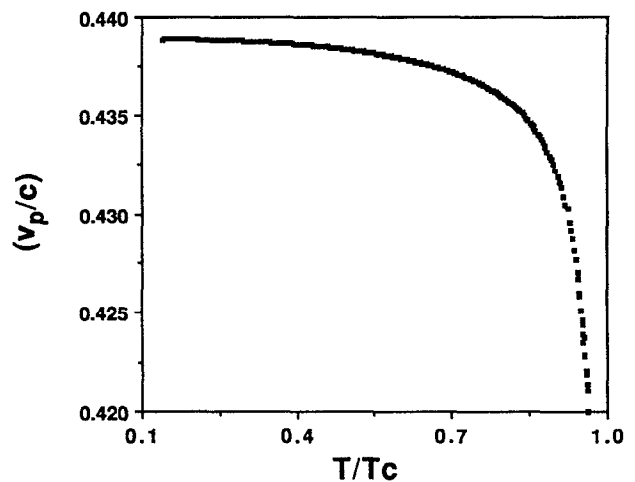


FIG. 3. Typical phase velocity data (normalized to the speed of light) obtained for a  $\text{YBa}_2\text{Cu}_3\text{O}_{7-\delta}$  superconducting microstrip resonator plotted vs temperature.

by this method is complicated by dielectric and radiation losses, and by the nontrivial analysis necessary to account for the two-dimensional geometry and finite film thickness. Details on the loss analysis of microstrip lines, along with experimental results, will be presented elsewhere.<sup>33</sup>

#### IV. DATA ANALYSIS

Here we discuss how the temperature dependence and magnitude of the penetration depth are obtained from the phase velocity data. The phase velocity depends on the penetration depth as shown in Eq. (3). In order to obtain  $\lambda$  by inverting Eq. (3) one must know the film and dielectric thicknesses as well as the effective dielectric constant of the transmission line,  $\epsilon_{\text{eff}}$ . The effective dielectric constant is the most difficult quantity to measure in our implementation of the microstrip resonator technique. Mason and Gould<sup>28</sup> and Henkels and Kircher<sup>29</sup> were able to determine the dielectric constant directly through measurements of the microstrip capacitance at low frequencies. However, because the thicknesses of the anodized dielectrics used in those studies were on the order of 1000  $\text{\AA}$ , their capacitance values (10–100 nF) are more than three orders of magnitude larger than those of the flip-chip microstrip lines studied here. In the case of the flip-chip microstrip, a capacitive determination of the dielectric constant proved inadequate to allow an accurate determination of the penetration depth. The use of high quality multilayer high- $T_c$  superconducting thin films to construct a monolithic microstrip structure should alleviate this problem in the future. Nevertheless, we developed two complementary techniques to analyze the data. One method obtains the temperature dependence of  $\lambda$  at low temperatures directly from the measured data, while the other uses a self-consistent fit of the data to an assumed penetration depth temperature dependence to obtain absolute values of  $\lambda$ .

## A. Low-temperature dependence of $\lambda(T)$

We can extract the temperature dependence of  $\lambda(T)$  at low temperatures from the phase velocity data without making assumptions about the magnitude of  $\lambda(T)$  or imposing a theoretical temperature dependence on the data. The analysis is also independent of the microstrip geometry and dielectric parameter ( $t, d, w, \epsilon_{\text{eff}}$ ).<sup>35-39</sup> Using Eq. (3) we derive the expression

$$\begin{aligned} & \ln \left[ \left( \frac{c}{v_p(T)} \right)^2 - \left( \frac{c}{v_p(T_m)} \right)^2 \right] \\ &= \ln \left[ \lambda(T) \coth \left( \frac{t}{\lambda(T)} \right) - \lambda(T_m) \coth \left( \frac{t}{\lambda(T_m)} \right) \right] \\ & \quad + \ln \left( \frac{2\epsilon_{\text{eff}}}{d} \right), \end{aligned} \quad (4)$$

where  $T_m$  is some low-temperature baseline temperature. For thick films, such that  $t > (3\lambda/2)$ , the hyperbolic cotangent is approximately unity. Thus, under this assumption and restricting ourselves to temperatures  $T < T_c/2$ , we obtain

$$\ln \left[ \left( \frac{c}{v_p(T)} \right)^2 - \left( \frac{c}{v_p(T_m)} \right)^2 \right] = \ln \left( \frac{\lambda(T)}{\lambda(T_m)} - 1 \right) + b, \quad (5)$$

where  $b$  is a nominally temperature-independent constant that depends on  $\lambda(T_m)$ ,  $\epsilon_{\text{eff}}$ ,  $t$ , and  $d$ . On the other hand, for thin films, such that  $t < (\lambda/2)$ , the hyperbolic cotangent can be approximated as  $(\lambda/t)$ . In this case the first natural logarithm on the right-hand side of Eq. (4) becomes  $\ln\{[\lambda^2(T) - \lambda^2(T_m)]/t\}$ , which can be approximated by  $\ln[\lambda(T)/\lambda(T_m) - 1]$  plus a temperature-independent constant, since the penetration depth does not change much from its low-temperature baseline temperature value for  $T < T_c/2$ . Thus, Eq. (5) holds for both thin and thick films such that  $t > (3\lambda/2)$  or  $t < (\lambda/2)$  in the low-temperature limit,  $T < T_c/2$ . For  $\text{YBa}_2\text{Cu}_3\text{O}_{7-\delta}$ , the zero temperature penetration depth is on the order of 1500 Å, so this analysis is valid for films with thickness less than 750 Å or greater than 2250 Å. The  $\text{YBa}_2\text{Cu}_3\text{O}_{7-\delta}$  films discussed here have thicknesses greater than 4000 Å, so Eq. (5) is valid. Equation (5) shows that the phase velocity data can be arranged such that its temperature dependence is solely that of the penetration depth at low temperatures. One implicit assumption is that the geometry, dielectric properties, and losses of the microstrip resonator do not affect the temperature dependence of the phase velocity. This assumption will be discussed in Sec. V. As we will see, the largest problem arises with respect to the temperature dependence of  $\epsilon_{\text{eff}}$ .

The low-temperature dependence of  $\lambda(T)$  simply measures the low-lying pair-breaking excitations that deplete the density of superconducting electrons. The low-temperature dependence of presently known superconductors usually takes one of two forms.<sup>1,3</sup> For a superconductor with a finite energy gap over the entire Fermi surface of minimum value  $\Delta(0)$ , the low-temperature dependence ( $T < T_c/2$ ) is given by<sup>40</sup>

$$\left( \frac{\lambda(T)}{\lambda(0)} - 1 \right) \propto \frac{1}{\sqrt{T}} \exp[-\Delta(0)/k_B T]. \quad (6)$$

Using Eq. (5) we see that the phase velocity data can be plotted as

$$\ln \left[ \left( \frac{c}{v_p(T)} \right)^2 - \left( \frac{c}{v_p(0)} \right)^2 \right] \approx \left( \frac{-\Delta(0)}{k_B T_c} \right) \frac{T_c}{T} + b, \quad (7)$$

where  $b$  varies slowly with temperature compared to the first term on the right hand side. Since the temperature dependence of Eq. (7) is dominated by the  $(1/T)$  term, a plot of the phase velocity data in the form of Eq. (7) vs  $T_c/T$  will approximate a straight line with slope  $-\Delta(0)/k_B T_c$  at low temperatures if the superconducting film has a finite energy gap over the entire Fermi surface of minimum value  $\Delta(0)$ . The baseline temperature in this case is  $T_m = 0$  K;  $v_p(0)$  is obtained by extrapolation from the lowest temperature data (2–4 K). Representative data for low- $T_c$  and high- $T_c$  films and the BCS theoretical prediction in the weak coupling limit [ $2\Delta(0)/k_B T_c = 3.5$ ] is plotted in this fashion in Fig. 4(a). The slopes of the lines in Fig. 4, as well as their shape, are only slightly sensitive to the choice of  $v_p(0)$ .

Another observed low-temperature dependence for  $\lambda(T)$  in superconductors is that associated with nodes in the superconducting energy gap, and has the form<sup>1,3</sup>

$$\left( \frac{\lambda(T)}{\lambda(0)} - 1 \right) \propto \left( \frac{T}{T_c} \right)^n. \quad (8)$$

Using Eq. (5) we see that the phase velocity data can be plotted as

$$\ln \left[ \left( \frac{c}{v_p(T)} \right)^2 - \left( \frac{c}{v_p(0)} \right)^2 \right] = n \ln \left( \frac{T}{T_c} \right) + \text{const.} \quad (9)$$

In this case, a plot of the phase velocity in the form of Eq. (9) vs  $\ln(T/T_c)$  will approximate a straight line with slope equal to the power law exponent,  $n$ , at low temperatures. To test for this possibility, the data in Fig. 4(a) are replotted in Fig. 4(b) over the same temperature range, but now as a function of  $\ln(T/T_c)$ .

## B. Absolute penetration depth

While the analysis above is very useful in determining the low temperature dependence of  $\lambda(T)$  without fitting the data, it does not tell us anything about  $\lambda$  at higher temperatures, nor does it give us absolute values of  $\lambda$ . The absolute value of  $\lambda$  over the entire temperature range can be obtained by inverting Eq. (3) to obtain the penetration depth from the phase velocity data once the effective dielectric constant of the microstrip line is determined. However, as explained previously, we are unable to directly measure the effective dielectric constant with sufficient accuracy. Analytic expressions to calculate  $\epsilon_{\text{eff}}$  are also not very useful since these formulas are typically only accurate to about 5%.<sup>25</sup> Because of these difficulties, we have developed an analysis technique that allows us to obtain  $\epsilon_{\text{eff}}$  from the phase velocity data itself by self-consistently fitting the data to an assumed penetration depth temperature

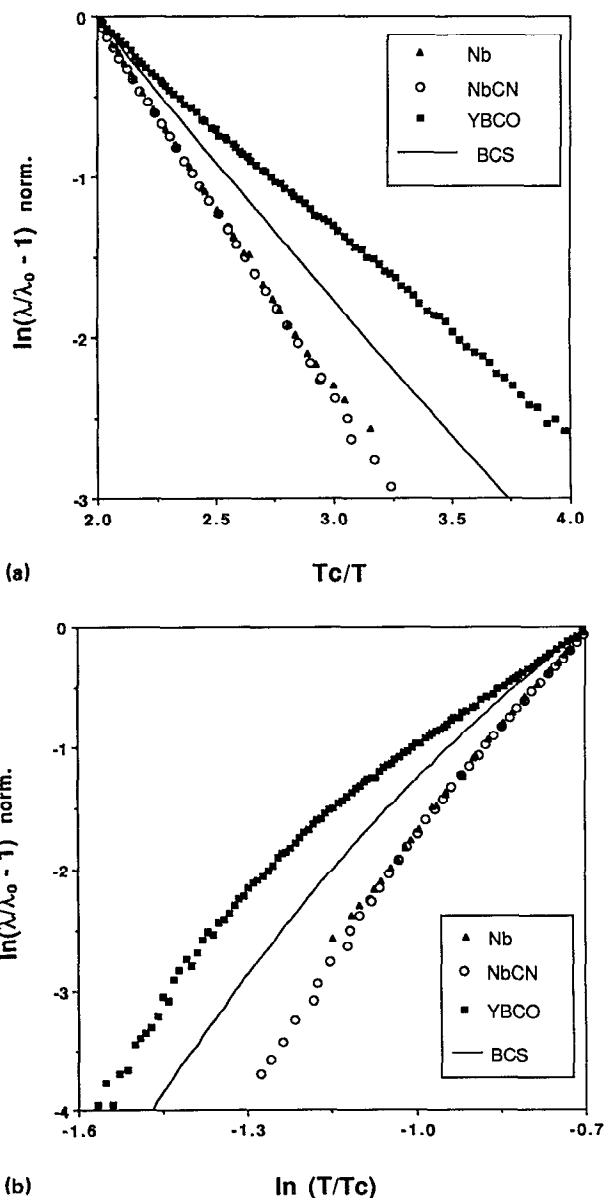


FIG. 4. (a) The phase velocity data for Nb, NbCN, and  $\text{YBa}_2\text{Cu}_3\text{O}_{7-s}$  films is plotted vs  $T_c/T$ , as suggested by Eq. (7), for reduced temperatures from 0.25 to 0.5. The low-temperature slope of these plots can be interpreted as the energy gap of an exponentially activated  $\lambda(T)$ . The result obtained for weak-coupled BCS theory is also shown (Ref. 42). (b) The same data now plotted vs  $\ln(T/T_c)$ , as suggested by Eq. (9), for the same temperature range. The low-temperature slope of these plots can be interpreted as the exponent,  $n$ , of a power law  $\lambda(T)$  temperature dependence. Note that both plots are normalized at  $T/T_c = 0.5$ .

dependence. Note that the deduced absolute values of  $\lambda$  are strongly dependent on the form of the temperature dependence assumed. This difficulty is not unique to our measurement technique; for example, dc magnetization measurements rely on similar fits to obtain absolute values of  $\lambda$ .<sup>41</sup>

We will briefly outline the procedure here; a more detailed description can be found in the following references.<sup>21,33</sup> Equation (3) can be rearranged as

$$\left(\frac{c}{v_p(T)}\right)^2 = \epsilon_{\text{eff}} + \left(\frac{2\epsilon_{\text{eff}}}{d}\right)\lambda_0 Z\left(\frac{T}{T_c}\right)M(T), \quad (10)$$

where we have written the penetration depth in terms of its zero temperature value  $\lambda_0$  and a normalized penetration depth  $Z(T/T_c) \equiv \lambda(T/T_c)/\lambda_0$ . We have also defined the factor

$$M(T) = \frac{1}{2} \left[ \coth\left(\frac{t_s}{\lambda(T)}\right) + g_c \operatorname{csch}\left(\frac{t_s}{\lambda(T)}\right) + \coth\left(\frac{t_g}{\lambda(T)}\right) \right], \quad (11)$$

which takes the two-dimensional microstrip geometry and finite film thicknesses into account and allows us to linearize the equation and simplify the computation. The phase velocity data are plotted as  $(c/v_p)^2$  vs  $Z(T)M(T)$  for a given  $T_c$ , where the normalized penetration depth  $Z(T)$  is theoretically calculated. Since  $M(T)$  depends on the unknown  $\lambda$  values as shown in Eq. (11), we initially assume that  $M(T) = 1$  for all  $T$ . Equation (10) shows that the slope of a linear least square fit of the data when plotted in this manner is proportional to  $\lambda_0$ , while the intercept is equal to  $\epsilon_{\text{eff}}$ . Once  $\epsilon_{\text{eff}}$  is determined, Eq. (3) can be inverted to directly obtain penetration depth values. The factor  $M(T)$  can now be calculated using these penetration depth values and measured film and dielectric thicknesses. The above steps then are repeated until  $M(T)$  converges. At this point the entire procedure is repeated interactively, varying  $T_c$  until the best linear least square fit is achieved.  $T_c$  values obtained in this manner agree very well with those obtained from dc resistivity measurements.

The analysis procedure outlined above results in  $\lambda(T)$  values calculated from the phase velocity data using Eq. (3) and the effective dielectric constant value obtained from the best fit. We call this the “data penetration depth curve.” The procedure also results in  $\lambda(T)$  values obtained by multiplying the zero temperature penetration depth value obtained from the best fit,  $\lambda_0$ , by the assumed normalized penetration depth  $Z(T)$ . We call this the “fitted penetration depth curve.” When the assumed temperature dependence fits the data very well, these two penetration depth curves will be identical. Conversely, if the assumed temperature dependence does not fit the data very well, these two curves can be quite different.

The specific procedure that we have developed to obtain the absolute value of  $\lambda(T)$  over the entire temperature range is as follows. First, the data are fit to an assumed temperature dependence  $Z(T)$  calculated using weak-coupled BCS theory (taking the energy gap  $2\Delta(0)/k_B T_c$  as a variable, while the electronic mean free path  $l$ , the coherence length  $\xi_0$ , and the London penetration depth  $\lambda_L$  are determined independently).<sup>42</sup> We then change the form of  $Z(T)$  by adjusting the energy gap parameter until the “data” and “fit” penetration depth curves approach each other. Egloff, Raychaudhuri, and Rinderer<sup>43</sup> used BCS theory with the energy gap as an adjustable parameter to obtain accurate penetration depth values for lead. However, they did not use self-consistent fits of the theory to the penetration depth data in order to obtain the energy gap, but used gap values obtained from tunneling measurements. The procedure of varying the energy gap within

weak-coupled BCS calculations to model strong coupling superconductors has also been validated by Blocksdorf and Hasse.<sup>44</sup>

## V. MEASUREMENT RESOLUTION AND SYSTEMATIC ERRORS

The main advantage of the microstrip resonator technique over other methods of determining the penetration depth is that it is an extremely high resolution measurement. In this section we will quantify the resolution of our penetration depth measurements. We will also look at systematic errors that can arise in the penetration depth measurement. These errors are mainly due to the presence of losses, and thermal variations of the microstrip geometry and dielectric properties.

In order to look at the resolution and systematic errors in the determination of the penetration depth from the phase velocity data, we need to invert Eq. (3) and obtain an expression for  $\lambda$  in terms of measured quantities. Since most of our measurements are done using resonators that are fabricated in the wide line ( $w \gg d$ ) and thick film ( $t > 3\lambda/2$ ) limits, we will investigate the measurement resolution and systematic errors in this limit. For wide lines  $k = 1$  and  $g_c = 0$ , while for thick films  $\coth(t/\lambda) = 1$ . With these assumptions, we can invert Eq. (3) to obtain:

$$\lambda = \frac{d}{2} \left[ \frac{1}{\epsilon_{\text{eff}}} \left( \frac{c}{v_p} \right)^2 - 1 \right]. \quad (12)$$

It can be shown that for narrow lines and/or thin films the measurement resolution will increase and the magnitude of systematic errors will decrease since the line inductance for a given value of  $\lambda$  is increased in those limits.<sup>33</sup> Thus, using Eq. (12) for the measurement pathology analysis will give a conservative estimate of both measurement resolution and systematic errors.

### A. Measurement resolution

The resolution in  $\lambda$  is limited by the resolution to which changes in the phase velocity can be measured. An estimate of the minimum resolvable change in the phase velocity,  $\delta v_p$ , can be made as follows. The phase velocity is determined from the resonant frequency of the transmitted power versus frequency data. The transmitted power data consists of 801 discrete frequency data points with the resonance peak centered in a frequency window with a width chosen to be approximately  $3\Delta f_{3\text{ dB}}$ . Recall that  $\Delta f_{3\text{ dB}}$  is related to the resonance quality factor by  $Q = f_{\text{res}}/\Delta f_{3\text{ dB}}$ . Thus, the minimum resolvable fractional frequency change is

$$\frac{\delta f}{f} = \frac{3\Delta f_{3\text{ dB}}}{801f} = \frac{1}{267Q}$$

The minimum resolvable fractional phase velocity change is equal to the minimum resolvable fractional frequency change since  $v_p$  is linearly related to  $f_{\text{res}}$ . A conservative  $Q$  value for a typical microstrip resonator (dielectric thickness  $d = 0.5$  mil) is 1000, which gives a fractional  $v_p$  change of approximately  $\delta v_p/v_p = 4 \times 10^{-6}$ . Using Eq.

(12) it can be shown that the minimum resolvable penetration depth change corresponding to  $\delta v_p$  can be written as  $\delta\lambda \approx d(\delta v_p/v_p)$ . Using the numbers above the translates to a conservative penetration depth measurement resolution of approximately  $0.5 \text{ \AA}$ . This result is essentially independent of the dielectric thickness since  $Q \propto d$ . Thus we see that the microstrip resonator measurement allows a very high resolution measurement of the penetration depth, which is especially important at low temperatures where an exponentially activated penetration depth does not change very much with temperature.

### B. Transmission line losses

When the resonator is lossy, the resonator frequency of the microstrip line can be "pulled" down by the finite resonance  $Q$ . To see this, consider the familiar equation of motion for a damped harmonic oscillator which is sinusoidally driven,

$$m\ddot{x} + \beta\dot{x} + kx = F \cos(\omega t)$$

or

$$\ddot{x} + 2\lambda\dot{x} + \omega_0^2 x = A \cos(\omega t),$$

where  $\omega_0^2 = k/m$  is the undamped oscillation frequency and the damping parameter is  $2\lambda = \beta/m$ . If the damping is light enough ( $\lambda < \omega_0$ ), the system will undergo damped oscillations with an oscillation frequency reduced from its undamped value,

$$\omega_{\text{res}}^2 = \omega_0^2 - 2\lambda^2.$$

In terms of the oscillator  $Q = \omega_{\text{res}}/2\lambda$ , the oscillation frequency in the presence of damping is

$$\omega_{\text{res}}^2 = \omega_0^2 [1 + (1/2Q^2)]^{-1} \quad \text{or} \quad \omega_{\text{res}} \cong \omega_0 [1 - (1/4Q^2)].$$

Thus the fractional change in the oscillation frequency due to losses is

$$\frac{\omega_{\text{res}} - \omega_0}{\omega_0} \cong -\frac{1}{4Q^2}.$$

Such a shift in resonant frequency is significantly less than the measurement resolution with practical  $Q$  values ( $\delta f/f_0 \approx 1/267Q$ ). Hence we can neglect the effect of finite losses on the resonant frequency. The only exception to this conclusion will be near  $T_c$ , where losses may lead to  $Q$  values less than 50. However, this will influence the determination of the penetration depth only for temperatures  $T > 0.98T_c$ .<sup>33</sup>

The above analysis assumes that the inertial term  $m$  of the harmonic oscillator (analogous to the kinetic inductance of the microstrip resonator) is not affected by the presence of damping. This is true in superconducting transmission lines, at least up to signal power levels for which the film inductance does not change.<sup>34</sup> At higher power levels the film inductance will increase because of current induced depairing or flux entry, but these phenomena occur beyond the power levels used in the measurements discussed here. However, in normal metal transmission lines, the situation is very different because the skin depth

(and hence the inductance) depends directly on the conductivity.<sup>45</sup> One finds that in normal metal transmission line resonators,

$$\frac{\omega_{\text{res}} - \omega_0}{\omega_0} \cong -\frac{1}{2Q},$$

and the resonant frequency is significantly lowered.

### C. Thermal variations of transmission line parameters

As seen in Eq. (12), the penetration depth value depends on the dielectric thickness  $d$  and the effective dielectric constant  $\epsilon_{\text{eff}}$ . In this section we will look at the effect of temperature-dependent dielectric properties. Note that in the thick film ( $t > 3\lambda/2$ ) limit the penetration depth is independent of the film thickness variations.

If we assume deviations in the dielectric thickness and effective dielectric constant of  $\delta d$  and  $\delta\epsilon_{\text{eff}}$  respectively we can derive a fractional deviation in  $\lambda$  using Eq. (12):

$$\frac{\delta\lambda}{\lambda} = \left( \frac{\delta d}{d} \right) - \frac{d}{2\lambda} \left( \frac{\delta\epsilon_{\text{eff}}}{\epsilon_{\text{eff}}} \right). \quad (13)$$

However, before moving on to temperature dependencies, simply look at how a temperature-independent error in the determination of  $d$  or  $\epsilon_{\text{eff}}$  affects the penetration depth values obtained. The dielectric thickness  $d$  is set by the thickness of the dielectric sheets, which is measured with an accuracy of approximately  $\pm 5\%$ . This implies a fractional deviation of  $\pm 5\%$  in the absolute value of the penetration depth (for  $\text{YBa}_2\text{Cu}_3\text{O}_{7-\delta}$   $\lambda \sim 1500 \text{ \AA}$ , and  $\delta\lambda \sim 75 \text{ \AA}$ ). However, since  $\delta\lambda$  scales with  $\lambda$ , a temperature-independent error in  $d$  will not affect the determination of the temperature dependence,  $\lambda(T)/\lambda_0$ , of the penetration depth. An error in the determination of the effective dielectric constant is more problematic for two reasons: (1) the prefactor ( $d/2\lambda$ ) in the above equation can be very large at low temperatures ( $\sim 50$ ), and (2) the error in the penetration depth,  $\delta\lambda$ , does not scale with  $\lambda$ , which implies that the temperature dependence as well as the absolute magnitude of  $\lambda$  will be affected. This is why analytical formulas using tabulated dielectric constant values (accuracy  $\sim 5\%$ ) or measurements of the low frequency capacitance cannot be used to determine the effective dielectric constant with sufficient accuracy to allow the determination of the penetration depth.

Next consider the effects of a temperature-dependent dielectric thickness  $d$ , film thickness  $t$ , or effective dielectric constant  $\epsilon_{\text{eff}}$ . These variations will have an effect on  $\lambda$  given by Eq. (13). Let us consider a temperature dependent dielectric thickness first. The low-temperature thermal expansion coefficient of Teflon FEP is  $\alpha \sim 1.4 \times 10^{-5} / \text{K}$ ,<sup>31</sup> which has the largest thermal expansion coefficient of any of the dielectrics used in the resonators.<sup>33</sup> The cumulative error in the penetration depth over a measurement temperature range  $\Delta T$  is given by  $\delta\lambda \approx \lambda_0 \alpha \Delta T$ . For  $\text{YBa}_2\text{Cu}_3\text{O}_{7-\delta}$  ( $\lambda_0 \sim 1500 \text{ \AA}$  and  $\Delta T \sim 90 \text{ K}$ ) this implies  $\delta\lambda \sim 2 \text{ \AA}$ , while for Nb ( $\lambda_0 \sim 750 \text{ \AA}$  and  $\Delta T \sim 9 \text{ K}$ )  $\delta\lambda \sim 0.1 \text{ \AA}$ . Since the measurement resolution is on the

order of  $1 \text{ \AA}$  or less, the effect of a temperature-dependent dielectric thickness can be ignored.

Although the penetration depth analysis is independent of film thickness in the thick film limit, changes in the film thickness have a similar effect on the penetration depth as the dielectric thickness if we use the relevant equations for the thin film limit. The thermal expansion coefficient of  $\text{YBa}_2\text{Cu}_3\text{O}_{7-\delta}$ , and other typical superconducting materials, at low temperatures should be much less than its room temperature value of approximately  $10^{-5} / \text{K}$ .<sup>46</sup> This expansion coefficient leads to cumulative  $\delta\lambda$  values similar to those shown above, and can therefore be ignored.

Finally, the effect of a temperature-dependent effective dielectric constant is considered. Because of the two-dimensional field distribution in the microstrip geometry (e.g., see Fig. 7 of Ref. 47), electric fields are not confined entirely to the dielectric between the strip and ground plane films. Thus the effective dielectric constant depends on the temperature-dependent dielectric constants of both the sheet dielectric and the substrate on which the strip conductor is deposited. For typical resonator geometries ( $w/d \sim 5-10$ ) and substrates such as MgO ( $\epsilon_r \sim 10$ ),  $\text{LaAlO}_3$  ( $\epsilon_r \sim 25$ ), yttria-stabilized zirconia (YSZ) ( $\epsilon_r \sim 25$ ), or sapphire ( $\epsilon_r \sim 10$ ), which have dielectric constants significantly larger than that of the sheet dielectric (for Teflon,  $\epsilon_r \sim 2$ ), analytic formulas<sup>25</sup> indicate that the temperature dependence of the substrate should dominate the temperature dependence of  $\epsilon_{\text{eff}}$ . This assumes that the temperature dependence of  $\epsilon_r$  for Teflon (we have no data for temperatures below 100 K) is not much larger than that of the substrates. We have estimated the value of  $\Delta\epsilon_r/\epsilon_r$  at low temperature for the above substrates: MgO,  $\text{LaAlO}_3$ , and sapphire ( $\Delta\epsilon_r/\epsilon_r < 1 \times 10^{-5} / \text{K}$ ),<sup>48,49</sup> and YSZ ( $\Delta\epsilon_r/\epsilon_r \sim 2 \times 10^{-4} / \text{K}$ ).<sup>48,49</sup> The estimate for MgO,  $\text{LaAlO}_3$ , and sapphire is believed to be an upper limit since the  $\epsilon_r(T)$  curves for these materials become very flat at low temperatures. The magnitude of  $\Delta\epsilon_r/\epsilon_r$  for YSZ is much larger than that of the other substrates, and stays relatively constant up to  $\sim 100 \text{ K}$ .<sup>49</sup>

Figure 5 shows the resonant frequency data for a microstrip resonator fabricated using  $\text{YBa}_2\text{Cu}_3\text{O}_{7-\delta}$  films on YSZ. The temperature dependence of the resonant frequency is clearly dominated by the linear temperature dependence of YSZ at low temperatures. The slope of a linear fit to the data at low temperatures ( $1.05 \times 10^{-4} / \text{K}$  as shown in Fig. 5) can be used to estimate  $\Delta\epsilon_r/\epsilon_r$  for YSZ. If the resonant frequency change is due solely to  $\epsilon_r(T)$  of the film substrate, then  $\Delta f_{\text{res}}/f_{\text{res}} = \Delta v_p/v_p = 0.5 \Delta\epsilon_r/\epsilon_r$ , and the fit obtained from the  $f_{\text{res}}(T)$  data implies  $\Delta\epsilon_r/\epsilon_r = 2.1 \times 10^{-4} / \text{K}$  for YSZ. This is in very good agreement with independent measurements.<sup>49</sup> Obviously, superconducting films deposited on substrates with very highly temperature-dependent dielectric constants, such as YSZ or  $\text{SrTiO}_3$ ,<sup>15</sup> are not well suited for  $\lambda(T)$  measurements using this technique. The effect of dielectric temperature dependencies on measurements using films deposited on MgO,  $\text{LaAlO}_3$ , or sapphire is much less, as seen in the data for a resonator fabricated using  $\text{YBa}_2\text{Cu}_3\text{O}_{7-\delta}$  films on MgO (Fig. 5).

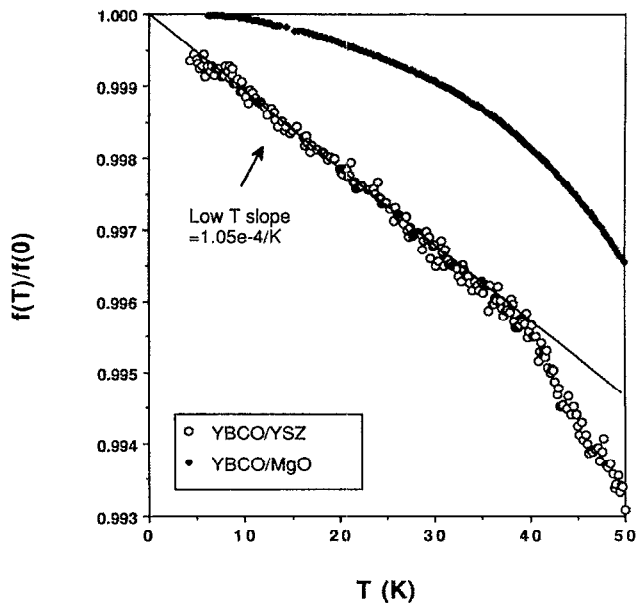


FIG. 5. The low-temperature resonant frequency data (normalized to its extrapolated zero temperature value) is shown here for two superconducting resonators. The data for the resonator fabricated using  $\text{YBa}_2\text{Cu}_3\text{O}_{7-\delta}$  films on YSZ clearly shows the effect of the temperature-dependent dielectric constant of YSZ, while the data for the resonator fabricated using  $\text{YBa}_2\text{Cu}_3\text{O}_{7-\delta}$  films on MgO show no temperature-dependent dielectric effects.

We can estimate the magnitude of the cumulative change in penetration depth over a measurement range  $\Delta T$  using  $\delta\lambda < (1 \times 10^{-5}/\text{K}) d \Delta T/2$ , which is obtained from Eq. (13). For  $\text{YBa}_2\text{Cu}_3\text{O}_{7-\delta}$  ( $d \sim 6.35 \mu\text{m}$  and  $\Delta T \sim 90 \text{ K}$ ) this implies  $\delta\lambda < 30 \text{ \AA}$ , while for Nb ( $d \sim 6.35 \mu\text{m}$  and  $\Delta T \sim 9 \text{ K}$ )  $\delta\lambda < 3 \text{ \AA}$ . The effect of a temperature dependent  $\epsilon_{\text{eff}}$  on low  $T_c$  films is not very large due to the small measurement temperature range, as is borne out by the fact that measurements of the temperature dependence of the penetration depth of Nb and NbCN films on sapphire substrates are in very good agreement with theory (see the following section). On the other hand, the effect of a temperature-dependent  $\epsilon_{\text{eff}}$  on high  $T_c$  films such as  $\text{YBa}_2\text{Cu}_3\text{O}_{7-\delta}$  is larger, although the estimate above is an upper limit. To put a cumulative penetration depth deviation over the full temperature range of  $\sim 30 \text{ \AA}$  into perspective, note that a conventional weak-coupled BCS superconductor with  $\lambda_0 \sim 1500 \text{ \AA}$ ,  $2\Delta(0)/k_B T_c = 3.5$  and  $T_c = 90 \text{ K}$  has a theoretically calculated<sup>42</sup> penetration depth which changes by more than  $2800 \text{ \AA}$  from  $T = 0$  to  $85 \text{ K}$ . We have also conducted detailed systematic experiments that verify that the change of the resonant frequency with temperature of our  $\text{YBa}_2\text{Cu}_3\text{O}_{7-\delta}$  resonators is consistent with  $\lambda(T)$  being the only temperature-dependent parameter.<sup>33</sup> This gives us confidence that our penetration depth measurements are not being affected by temperature-dependent dielectric properties, or any other parasitic temperature dependence.

## VI. EXPERIMENTAL RESULTS

In this section we will present some experimental results obtained using the microstrip resonator technique. Since the focus of this article is the measurement technique itself we will be brief; a more detailed account of the results of our penetration depth measurements of both high- and low- $T_c$  films can be found in Refs. 21, 33, and 35–39.

The results presented here were obtained for Nb, NbCN, and  $\text{YBa}_2\text{Cu}_3\text{O}_{7-\delta}$  thin films. The Nb films used were sputtered<sup>50</sup> on sapphire 1-102 substrates, and had low residual resistivity ratios ( $\approx 4$ ), but high  $T_c$  ( $\sim 9.2 \text{ K}$ ). These films were  $3650 \text{ \AA}$  thick. The NbCN films were prepared at TRW by reactive sputtering on sapphire substrates,<sup>50</sup> were  $5660 \text{ \AA}$  thick, and had  $T_c \sim 16 \text{ K}$ .  $\text{YBa}_2\text{Cu}_3\text{O}_{7-\delta}$  films were prepared at Stanford by *in-situ* off-axis sputtering<sup>51</sup> on MgO, YSZ, and  $\text{LaAlO}_3$  substrates. These  $\text{YBa}_2\text{Cu}_3\text{O}_{7-\delta}$  films are *c*-axis normal oriented and heavily twinned, implying that the shielding currents used to measure the penetration depth flow roughly equally in the *a* and *b* directions. These films also show high critical current densities<sup>52</sup> and good rf properties.<sup>53,54</sup> The  $\text{YBa}_2\text{Cu}_3\text{O}_{7-\delta}$  films used in the measurements presented here were sputtered to a thickness of  $4340 \text{ \AA}$  on MgO, and had  $T_c \sim 82 \text{ K}$  as determined from dc resistivity measurements.

Microstrip resonators were fabricated using these superconducting thin films. The width,  $w$ , of the patterned strip conductor was  $103$ ,  $75$ , and  $47 \mu\text{m}$  for the Nb, NbCN, and  $\text{YBa}_2\text{Cu}_3\text{O}_{7-\delta}$  thin films, respectively. All of the resonators used a  $12.7\text{-}\mu\text{m}$ -thick Teflon FEP<sup>31</sup> sheet as the dielectric, and were measured using the experimental procedure outlined in Sec. III. Representative phase velocity versus temperature data is shown in Fig. 3.

The low-temperature dependence of  $\lambda(T)$  can be investigated directly, as discussed in Sec. IV A. When the phase velocity data is plotted as suggested by Eq. (7), the exponential temperature dependence should make the data fall on a line with slope  $-\Delta(0)/k_B T_c$ . Figure 4(a) shows that the films follow this low-temperature exponential dependence to a very good approximation. The plots for the Nb and NbCN films show an inferred energy gap of  $2\Delta(0)/k_B T_c = 4.4 \pm 0.5$  and  $4.8 \pm 0.5$ , respectively, while the plot for the  $\text{YBa}_2\text{Cu}_3\text{O}_{7-\delta}$  film shows an inferred energy gap of  $2\Delta(0)/k_B T_c = 2.5 \pm 0.2$ . We are more confident about the value deduced for  $\text{YBa}_2\text{Cu}_3\text{O}_{7-\delta}$  since those data extend down to lower reduced temperatures ( $T/T_c$ ) than do the NbCN or Nb data. In Fig. 4(b) the phase velocity data are plotted as suggested by Eq. (9), which allows one to check for power law behavior in the low-temperature penetration depth. The data for all of the films (as well as BCS weak-coupled theory) show a slight but distinct downward curvature, which is consistent with what we would expect for an exponentially activated penetration depth. If we ignore this curvature, we can obtain values of the power law exponent for the temperature dependence of  $\lambda$  on the films: for the Nb film  $n \sim 6.0$ , for the NbCN film  $n \sim 6.5$ , and for the YBCO film,  $n \sim 3.5$ . Of course, given that the data are better fit by an exponential temperature dependence, the physical significance of these

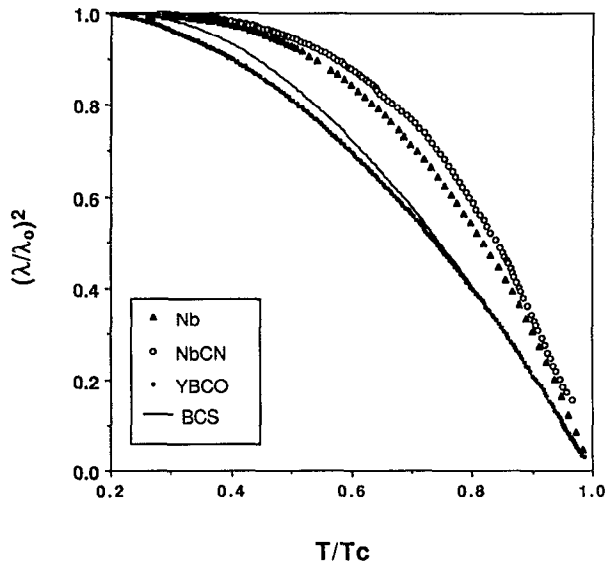


FIG. 6. The penetration depth curves obtained for the Nb, NbCN, and  $\text{YBa}_2\text{Cu}_3\text{O}_{7-\delta}$  films from fits of the phase velocity to assumed temperature dependencies is presented above as plots of  $[\lambda(0)/\lambda(T)]^2$  vs  $T/T_c$ . We also show the result calculated from weak-coupled BCS theory.<sup>42</sup>

exponents is dubious. The low-temperature penetration depth results are summarized in Table I.

The data can also be analyzed to obtain absolute values of  $\lambda$  by the self-consistent fitting method described in Sec. IV B. Figure 6 shows the “data” penetration depth curves obtained for the Nb, NbCN, and  $\text{YBa}_2\text{Cu}_3\text{O}_{7-\delta}$  films described above. The results are presented as curves of  $[\lambda_0/\lambda(T)]^2$  vs  $(T/T_c)$  in order to emphasize the effect of the energy gap parameter  $2\Delta(0)/k_B T_c$  near  $T_c$ . The data for the Nb film can be self-consistently fit to a BCS temperature dependence with an energy gap parameter  $2\Delta(0)/k_B T_c = 4.2 \pm 0.25$ ,<sup>55</sup> giving a zero temperature penetration depth  $\lambda_0 = 860 \text{ \AA}$  (Table I), which agrees very well with the value of  $825 \text{ \AA}$  calculated using BCS theory.<sup>42,55</sup> Although the energy gap parameter obtained for the Nb film is slightly higher than values obtained from tunneling experiments,  $2\Delta(0)/k_B T_c = 3.8\text{--}3.9$ ,<sup>56,57</sup> it is in-

TABLE I. The penetration depth results for the Nb, NbCN, and  $\text{YBa}_2\text{Cu}_3\text{O}_{7-\delta}$  films measured are summarized here. The parameters  $2\Delta/kT_c$  of an exponential low temperature  $\lambda(T)$  and  $n$  of a power law low-temperature  $\lambda(T)$  were inferred from Figs. 4(a) and 4(b). Results of the self-consistent fitting of the data to a BCS temperature dependence where the energy gap parameter is varied are also shown. Since the  $\text{YBa}_2\text{Cu}_3\text{O}_{7-\delta}$  data could not be self-consistently fit to a single gap BCS temperature dependence over the entire temperature range we have shown the result obtained for a self-consistent fit of that data over the temperature range  $T > 0.65T_c$ .

Film	Low temperature $\lambda(T)$		Self-consistent $\lambda(T)$ fit	
	Inferred $2\Delta/kT_c$	Inferred $n$	$2\Delta/kT_c$	$\lambda_0(\text{\AA})$
Nb	$4.4 \pm 0.5$	$\sim 6.0$	$4.2 \pm 0.25$	860
NbCN	$4.8 \pm 0.5$	$\sim 6.5$	$4.75 \pm 0.25$	2820
$\text{YBa}_2\text{Cu}_3\text{O}_{7-\delta}$	$2.5 \pm 0.2$	$\sim 3.5$	$4.5 \pm 0.2$	1700

teresting to note that Sheen *et al.*,<sup>58</sup> have recently fit surface resistance values obtained from a Nb stripline resonator measurement to BCS theory with  $2\Delta(0)/k_B T_c = 4.4$ . The NbCN film can also be self-consistently fit to a BCS temperature dependence, with  $2\Delta(0)/k_B T_c = 4.75 \pm 0.25$  (Ref. 55) and  $\lambda_0 = 2820 \text{ \AA}$  (Table I). We have no independent data for the energy gap of NbCN, although we might expect that it is close to the value for NbN, which ranges from  $2\Delta(0)/k_B T_c \sim 4.3$  obtained by tunneling measurements<sup>59</sup> and  $2\Delta(0)/k_B T_c = 4.75 \pm 0.25$  obtained from NbN stripline resonator surface resistance measurements.<sup>60</sup> Measurements of the zero temperature penetration depth of NbCN films give values ranging from 2370 to 3030  $\text{\AA}$ .<sup>61</sup>

On the other hand, the  $\text{YBa}_2\text{Cu}_3\text{O}_{7-\delta}$  data cannot be self-consistently fit to a BCS temperature dependence with a single energy gap parameter over the entire temperature range. For example, a fit of the data to a standard weak-coupled BCS temperature dependence [ $2\Delta(0)/k_B T_c = 3.5$ ] (Ref. 55) resulted in a zero temperature penetration depth value of  $\lambda_0 = 1300 \text{ \AA}$ . However, the lack of self-consistency can be seen in Fig. 6 where the penetration depth curve obtained from the fitting of the data and the assumed BCS penetration depth curve are both plotted. At lower reduced temperatures, the  $\text{YBa}_2\text{Cu}_3\text{O}_{7-\delta}$  penetration depth curve changes faster with temperature than the BCS theory, which is consistent with the  $\text{YBa}_2\text{Cu}_3\text{O}_{7-\delta}$  film having an energy gap parameter smaller than 3.5 in that temperature range. This is in agreement with Fig. 4(a), where we saw that the low-temperature penetration depth of the  $\text{YBa}_2\text{Cu}_3\text{O}_{7-\delta}$  film is consistent with  $2\Delta(0)/k_B T_c \sim 2.5$ . On the other hand, we find that when we fit only the high temperature ( $0.65T_c$  to  $0.98T_c$ ) data, a self-consistent fit can be obtained for a single gap BCS temperature dependence with  $2\Delta(0)/k_B T_c = 4.5$  and  $\lambda_0 = 1700 \text{ \AA}$  (Table I). This is in good agreement with measurements of  $\lambda(T)$  restricted to the same temperature range in single crystal  $\text{YBa}_2\text{Cu}_3\text{O}_{7-\delta}$ ,<sup>18</sup> where it was found that a single gap BCS fit yields  $2\Delta(0)/k_B T_c = 4.3$ . Note that, as in any penetration depth measurement technique that obtains absolute  $\lambda$  values by fitting the data to an assumed temperature dependence, the  $\lambda_0$  value obtained is highly dependent on the assumed temperature dependence<sup>33</sup> and temperature region for which the data are fit.<sup>41</sup> Thus, we regard as questionable any  $\lambda_0$  value obtained from an inconsistent fit.

There are several possible interpretations of our  $\text{YBa}_2\text{Cu}_3\text{O}_{7-\delta}$  results. The results could correctly reflect the intrinsic behavior of the penetration depth in  $\text{YBa}_2\text{Cu}_3\text{O}_{7-\delta}$  thin films, which may not be well described by conventional BCS theory. We have also looked at a double-gap parallel superconductor model and a series weak-link model.<sup>39</sup> The first of these models assumes that the superconducting carriers can be characterized by two energy gaps, while the second assumes that the low temperature behavior of  $\lambda$  is dominated by weak links. Both of these models result in very good fits to the data and give zero temperature penetration depths of  $\lambda_0 = 1565$  and  $1440 \text{ \AA}$ , respectively.<sup>39</sup> Distinguishing between these two interpretations is the subject of current work.

## ACKNOWLEDGMENTS

We would like to acknowledge H. Sze, N. Switz, and Z. Ma for their contributions in the development of this measurement technique. We are also indebted to J. Halbritter, G. Deutscher, C. B. Eom, T. H. Geballe, H. J. Snortland, N. Bluzer, S. Whitmore, R. W. Simon, and R. Taber for many fruitful and stimulating discussions. This work was supported by the National Science Foundation (ECS) and the Strategic Defense Initiative Organization. One of the authors (BWL) was supported by a fellowship from Digital Equipment Corp. and by the Semiconductor Research Corporation.

- <sup>1</sup>See, for example, J. F. Annett, N. Goldenfeld, and S. R. Renn, in *Physical Properties of High Temperature Superconductors II*, edited by D. M. Ginsberg (World Scientific, NJ, 1990), p. 571.
- <sup>2</sup>J. F. Annett, N. Goldenfeld, and S. R. Renn, *Phys. Rev. B* (to be published).
- <sup>3</sup>D. Shoenberg, *Superconductivity* (Cambridge University Press, Cambridge, 1960), p. 147.
- <sup>4</sup>L. Krusin-Elbaum, R. L. Greene, F. Holtzberg, A. P. Malozemoff, and Y. Yeshurun, *Phys. Rev. Lett.* **62**, 217 (1989).
- <sup>5</sup>A. L. Schawlow and G. E. Devlin, *Phys. Rev.* **113**, 120 (1959).
- <sup>6</sup>S. Sridhar, D. H. Wu, and W. Kennedy, *Phys. Rev. Lett.* **63**, 1873 (1989).
- <sup>7</sup>E. Laurmann and D. Shoenberg, *Nature* **160**, 747 (1947); E. Laurmann and D. Shoenberg, *Proc. R. Soc. (London) A* **198**, 560 (1949).
- <sup>8</sup>A. T. Fiory, A. F. Hebard, P. M. Mankiewicz, and R. E. Howard, *Appl. Phys. Lett.* **52**, 2165 (1988).
- <sup>9</sup>A. T. Fiory, A. F. Hebard, P. M. Mankiewicz, and R. E. Howard, *Phys. Rev. Lett.* **61**, 1419 (1988).
- <sup>10</sup>S. Sridhar and W. L. Kennedy, *Rev. Sci. Instrum.* **59**, 531 (1988).
- <sup>11</sup>J. P. Turneaure and I. Weissman, *J. Appl. Phys.* **39**, 4417 (1968); C. Zahopoulos, W. L. Kennedy, and S. Sridhar, *Appl. Phys. Lett.* **52**, 2168 (1988).
- <sup>12</sup>S. Sridhar, *J. Appl. Phys.* **63**, 159 (1988).
- <sup>13</sup>A. M. Portis, D. W. Cooke, and E. R. Gray, *J. Supercond.* **3**, 297 (1990).
- <sup>14</sup>L. D. Chang, M. J. Moskowitz, R. B. Hammond, M. M. Eddy, W. L. Olsen, D. D. Casavant, E. J. Smith, M. Robinson, L. Drabeck, and G. Gruner, *Appl. Phys. Lett.* **55**, 1357 (1989).
- <sup>15</sup>L. Drabeck, J. P. Carini, G. Gruner, T. Hylton, K. Char, and M. R. Beasley, *Phys. Rev. B* **39**, 785 (1989).
- <sup>16</sup>N. Klein, H. Chaloupka, G. Muller, S. Orbach, H. Piel, B. Roas, L. Schultz, U. Klein, and M. Peiniger, *J. Appl. Phys.* **67**, 6940 (1990).
- <sup>17</sup>L. Drabeck, K. Holzer, G. Gruner, and D. J. Scalapino, *J. Appl. Phys.* **68**, 892 (1990).
- <sup>18</sup>B. W. Langley and J. Halbritter (unpublished).
- <sup>19</sup>S. Sridhar, D. H. Wu, and W. Kennedy, *Phys. Rev. Lett.* **63**, 1873 (1989).
- <sup>20</sup>R. Meserve and P. M. Tedrow, *J. Appl. Phys.* **40**, 2028 (1969).
- <sup>21</sup>S. M. Anlage, H. Sze, H. J. Snortland, S. Tahara, B. Langley, C. B. Eom, M. R. Beasley, and R. Taber, *Appl. Phys. Lett.* **54**, 2710 (1989).
- <sup>22</sup>S. M. Anlage, H. J. Snortland, and M. R. Beasley, *IEEE Trans. Magn. MAG-25*, 1388 (1989).
- <sup>23</sup>A. B. Pippard, *Proc. R. Soc. (London) A* **191**, 370 (1947).
- <sup>24</sup>K. Chang, *J. Appl. Phys.* **50**, 8129 (1979).
- <sup>25</sup>M. V. Schneider, *Bell Syst. Tech. J.* **48**, 1421 (1969).
- <sup>26</sup>A. B. Pippard, *Proc. R. Soc. (London) A* **191**, 399 (1947).
- <sup>27</sup>D. R. Young, J. C. Swihart, S. Tansal, and N. H. Meyers, *Solid-State Electron.* **1**, 378 (1960).
- <sup>28</sup>P. V. Mason and R. W. Gould, *J. Appl. Phys.* **40**, 2039 (1969).
- <sup>29</sup>W. H. Henkels and C. J. Kircher, *IEEE Trans. Magn. MAG-13*, 63 (1977).
- <sup>30</sup>R. C. Taber, *Rev. Sci. Instrum.* **61**, 2200 (1990).
- <sup>31</sup>Teflon Film Product Info, Bullentin E-67603, DuPont Corp. (1989).
- <sup>32</sup>X. D. Wu *et al.*, *Appl. Phys. Lett.* **56**, 400 (1990).
- <sup>33</sup>B. W. Langley, Ph.D. thesis, Stanford University (1991).
- <sup>34</sup>H. J. Snortland, S. M. Anlage, J. Halbritter, and M. R. Beasley, *Bull. Am. Phys. Soc.* **35**, 810 (1990).
- <sup>35</sup>S. M. Anlage, B. W. Langley, H. J. Snortland, C. B. Eom, T. H. Geballe, and M. R. Beasley, *J. Superconductivity* **3**, 311 (1990).
- <sup>36</sup>S. M. Anlage, B. W. Langley, J. Halbritter, S. Tahara, H. Sze, N. Switz, C. B. Eom, H. J. Snortland, R. Taber, T. H. Geballe, and M. R. Beasley, *Physica C* **162-164**, 1645 (1989).
- <sup>37</sup>S. M. Anlage, B. W. Langley, G. Deutscher, R. W. Simon, C. B. Eom, M. R. Beasley, and T. H. Geballe, proceedings of the 19th Low Temperature Physics Conference, Brighton, England (1990).
- <sup>38</sup>S. M. Anlage, B. Langley, J. Halbritter, T. Hylton, C. B. Eom, D. K. Fork, N. Switz, T. H. Geballe, and M. R. Beasley, proceedings of the Material Research Society Spring Meeting, San Francisco, CA (1990).
- <sup>39</sup>S. M. Anlage, B. W. Langley, G. Deutscher, J. Halbritter, and M. R. Beasley (unpublished).
- <sup>40</sup>J. Halbritter, *Z. Phys.* **243**, 201 (1971).
- <sup>41</sup>A. F. Hebard, A. T. Fiory, and D. R. Harshman, *Phys. Rev. Lett.* **62**, 2885 (1989); R. L. Greene, L. Krusin-Elbaum, and A. P. Malozemoff, *Phys. Rev. Lett.* **62**, 2886 (1989).
- <sup>42</sup>J. Halbritter, *Z. Phys.* **266**, 209 (1974); J. Halbritter, *Ext. Bericht 3*, 70-6 KFK Karlsruhe (1970).
- <sup>43</sup>C. Egloff, A. K. Raychaudhuri, and L. Rinderer, *Proceedings of the 17th International Low Temperature Physics Conference, LT-17 (Karlsruhe)*, edited by U. Eckern, A. Schmid, W. Weber, and H. Wuhl (North Holland, Amsterdam, 1984), p. 1033.
- <sup>44</sup>R. Blocksdorf and J. Hasse, *Z. Phys. B* **43**, 193 (1981).
- <sup>45</sup>P. Grivet, *The Physics of Transmission Lines at High and Very High Frequencies* (Academic, New York, 1970), p. 275.
- <sup>46</sup>R. L. Sandstrom, E. A. Giess, W. J. Gallagher, A. Segmuller, E. I. Cooper, M. F. Chisholm, A. Gupta, S. Shinde, and R. B. Laibowitz, *Appl. Phys. Lett.* **53**, 1874 (1988).
- <sup>47</sup>L. E. Alsop, A. S. Goodman, F. G. Gustavson, and W. L. Miranker, *J. Comput. Phys.* **31**, 216 (1979).
- <sup>48</sup>Y. Kobayashi, J. Sato, and K. Yajima, *Trans. IEIECE E* **72**, 290 (1989).
- <sup>49</sup>G. A. Samara, *J. Appl. Phys.* **68**, 4214 (1990).
- <sup>50</sup>The Nb and NbCN films were sputtered from Nb targets in Ar and Ar/N<sub>2</sub>/CH<sub>4</sub> atmospheres, respectively, by J. Murduck at TRW, Redondo Beach, CA.
- <sup>51</sup>C. B. Eom, J. Z. Sun, K. Yamamoto, A. F. Marshall, K. E. Luther, T. H. Geballe, and S. S. Laderman, *Appl. Phys. Lett.* **55**, 595 (1989).
- <sup>52</sup>S. Tahara, S. M. Anlage, J. Halbritter, C. B. Eom, D. K. Fork, T. H. Geballe, and M. R. Beasley, *Phys. Rev. B* **41**, 11 203 (1990).
- <sup>53</sup>C. B. Eom, J. Z. Sun, S. K. Streiffer, A. F. Marshall, K. Yamamoto, B. M. Lairson, S. M. Anlage, S. S. Laderman, R. Taber, and T. H. Geballe, *Physica C* **171**, 354 (1990).
- <sup>54</sup>S. S. Laderman, R. C. Taber, R. D. Jacowitz, J. L. Moll, C. B. Eom, T. L. Hylton, A. F. Marshall, T. H. Geballe, and M. R. Beasley, *Phys. Rev. B* **43**, 2922 (1991).
- <sup>55</sup>The theoretical BCS penetration depth temperature dependence is calculated (Ref. 42) with the following parameters: for Nb,  $T_c = 9$  K,  $I_{MFP} = 130$  Å,  $\lambda_L = 390$  Å and  $\xi_0 = (2/\pi)\xi_F = 380$  Å; for NbCN,  $T_c = 18$  K,  $I_{MFP} = 100$  Å,  $\lambda_L = 2300$  Å and  $\xi_0 = 50$  Å; and for YBa<sub>2</sub>Cu<sub>3</sub>O<sub>7- $\delta$</sub> ,  $T_c = 90$  K,  $I_{MFP} = 100$  Å,  $\lambda_L = 1400$  Å, and  $\xi_0 = 15$  Å.
- <sup>56</sup>S. I. Park, Ph.D. thesis, Stanford University (1986).
- <sup>57</sup>R. F. Broom and P. Wolf, *Phys. Rev. B* **16**, 3100 (1977).
- <sup>58</sup>D. M. Sheen, S. M. Ali, D. E. Oates, R. S. Withers, and J. A. Kong (unpublished).
- <sup>59</sup>S. Kubo, M. Asahi, M. Hikita, and M. Igarashi, *Appl. Phys. Lett.* **44**, 258 (1984).
- <sup>60</sup>D. E. Oates, A. C. Anderson, C. C. Chin, J. S. Derov, G. Dresselhaus, and M. S. Dresselhaus, *Phys. Rev. B* **43**, 7655 (1991).
- <sup>61</sup>J. S. Moodera, T. L. Francavilla, and S. A. Wolf, *IEEE Trans. Magn. MAG-23*, 1003 (1987).